Controlling the phase transformation of alumina for enhanced stability and catalytic properties

Sejin Jang[1], Dong Gun Oh[1], Haneul Kim[1], Kwang Hyun Kim[1], Konstantin Khivantsev[2]*, Libor Kovarik[2]*, and Ja Hun Kwak[1]*

[1]School of Energy and Chemical Engineering, Ulsan National Institute of Science and Technology (UNIST), 50 UNIST-gil, Ulsan 44919, Republic of Korea.

[2]Institute for Integrated Catalysis, Pacific Northwest National Laboratory, Richland, WA 99352, USA.

*Corresponding author E-mail address: Konstantin.Khivantsev@pnnl.gov;

Libor.Kovarik@pnnl.gov;

jhkwak@unist.ac.kr

Abstract

Current transition alumina catalysts require the presence of significant amounts of toxic, environmentally deleterious dopants for their stabilization. Herein, we report a simple and novel strategy to engineer transition aluminas to withstand aging temperatures up to 1200°C without inducing the transformation to low-surface-area α-alumina and without requiring dopants. By judiciously optimizing the abundance of dominant facets and the interparticle distance, we can control the temperature of the phase transformation from θ-alumina to α-alumina and the specific surface sites on the latter. These specific surface sites provide favorable interactions with supported metal catalysts, leading to improved metal dispersion and greatly enhanced catalytic activity for hydrocarbon oxidation. The results presented herein not only provide molecular-level insights into the critical factors causing deactivation and phase transformation of aluminas but also pave the way for the development of catalysts with excellent activity for catalytic hydrocarbon oxidation.

Introduction

Transition aluminas are critical materials for industrially important catalytic and environmental applications(*1-3*), with the total annual production reaching ~140 million metric tons. For industrial application, transition aluminas require the presence of dopants to stabilize their surface area (SA) and prevent their transformation into low-surface-area α-Al_2O_3(*4-6*), also known as corundum, under severe thermal stress conditions typically encountered in the industry. These conditions lead to the loss of catalytic and mechanical properties and the covering of active metal/oxide nanoparticles. For example, to prevent the transformation of high SA nanosized aluminas to low-SA α-Al_2O_3 at ~1050°C, significant amounts of dopants such as barium and rare-earths are added to aluminas(*4-6*). Unfortunately, these dopants are toxic and environmentally deleterious, and their use is obviously undesirable from a modern environmental perspective. They also affect the catalytic behavior of aluminas, hindering the precise determination of the active sites and a straightforward evaluation of the supported catalysts. Despite the significant advances made in understanding transition aluminas and their structure and surface(*1, 7-14*), including our work over the last two decade(*15*), the transformation of transition aluminas into α-Al_2O_3 is not well understood on a molecular-level. α-Al_2O_3 is formed at high temperatures from various metastable alumina precursors such as δ/θ-, θ-, and κ-Al_2O_3(*1, 16*). However, gaining insight into the phase transformation to α-Al_2O_3 is difficult because of the high-temperature, the presence of mixed phases, and the precipitously fast rate of transformation(*17-22*). Furthermore, the effect of the properties of the starting alumina on those of the final α-Al_2O_3 product, such as morphology, SA, and surface properties, and ultimately on its catalytic functions is not well understood. This understanding at a molecular-level could eventually lead to the development of approaches to mitigate

deactivation, extend thermal aging resistance, and potentially transform inactive materials into active ones(*23*).

Herein, we judiciously studied the effect of the surface properties and interparticle distance of the starting pure-phase θ-Al_2O_3 on the θ-to-α phase transformation and the characteristics of α-Al_2O_3 as a catalyst support. We devised a simple and scalable method that, to the best of our knowledge, has not been applied to alumina materials before: after the hydrothermal synthesis of uniform boehmite particles with a specific rod-like morphology as precursors of transition aluminas, we collected the solid particles by either centrifugation, oven drying, or freeze-drying, obtaining final alumina products with different dominant facets (between centrifugation and oven drying/freeze-drying) and average interparticle distances depending on the collection method. Pure θ-Al_2O_3 with the same rod-like morphology showed a significantly different phase transformation temperature to that of α-Al_2O_3 depending on the dominant facet. We successfully extended the thermal stability of transition alumina to 1200°C–1260°C even in the absence of any rare-earth dopants. X-ray diffraction (XRD), transmission electron microscopy (TEM), in situ TEM, and diffuse reflectance infrared Fourier transform spectroscopy (DRIFTS) analyses provided molecular-level insight into the transformation process and the factors affecting it.

Furthermore, DRIFTS and microscopy measurements revealed that the surfaces of θ- and α-Al_2O_3 prepared via this simple modification were different. This difference translates into notable differences in the ability of these alumina materials as catalyst supports to disperse metal particles, paving the way to novel catalytic materials with enhanced activity and thermal stability.

Results and Discussion

To provide molecular-level insight into the transformation of transition alumina to α-Al_2O_3, we prepared three pure rod-like θ-Al_2O_3 samples according to our previous reports(*24*). We selected pure θ-Al_2O_3 with a rod-like morphology to eliminate the crystalline phase effect on the phase transformation and synthesized the samples using the same protocols except for the drying method, i.e., centrifugation, oven drying, or freeze-drying. The resulting samples were denoted as Al_2O_3-C, Al_2O_3-O, and Al_2O_3-F, respectively. This simple, yet crucial synthetic step has not been investigated for transition aluminas to date due to the prevailing assumption that it has no bearing on the properties of the resulting material. However, we can now confirm its decisive role in the stability and activity of the prepared materials.

Figure S1–4 and Table S1 summarize detailed information about the samples. TEM observation clearly confirmed the formation of a uniform rod-like alumina crystal structure in the three cases (Figure 1a–c), and an XRD analysis demonstrated that thermal treatment at 1100°C for 10 h afforded a pure θ-Al_2O_3 phase (Figure 1d). The infrared (IR) spectra revealed significant differences in the OH stretching region between the three samples (Figure S4). Thus, the OH absorption band appearing at 3790 cm^{-1} in the spectrum of θ-Al_2O_3-C is much more intense than those observed in the spectra of θ-Al_2O_3-O and θ-Al_2O_3-F. In addition, the OH band at 3730 cm^{-1} is dominant for θ-Al_2O_3-C, whereas that at 3740 cm^{-1} prevails for θ-Al_2O_3-O and θ-Al_2O_3-F. A comparison of the IR spectra of θ-Al_2O_3-C and θ-Al_2O_3-O revealed the presence of similar bands but with a “mirror” abundance, which indicates that these samples preferentially expose different facets, that is, the facets abundant in θ-Al_2O_3-C are much less abundant in θ-Al_2O_3-O and vice versa, despite their identical XRD patterns (Figure 1e)(*9-12*). In fact, the high-resolution TEM (HRTEM) images showed the presence of rods that cluster

preferentially along the (100) facet, which provides better adhesion due to the centrifugal force, as typically observed for two-dimensional materials. For θ-Al_2O_3-C, the macroscopic (110) facet is the most abundant, although it is broken into nanosegments as we previously reported (hereinafter, this facet will be called reconstructed (110) for simplicity)(*25*). However, θ-Al_2O_3-O and θ-Al_2O_3-F do not show this behavior, and the (100) facet remains the most abundant one. This difference provides a unique opportunity for us to assign the OH bands to specific OH groups and facets. In particular, the (100) facets give rise to O_5Al(VI)–OH and O_3Al(IV)–OH bands at 3770 and 3745 cm^{-1}, respectively, whereas the reconstructed (110) facets of Al_2O_3-C produce O_5Al(VI)–OH and O_3Al(IV)–OH bands at 3790 and 3730 cm^{-1}, respectively(*25*). This is consistent with our initial assignment for alumina samples, where we suggested that the bands at 3770 and 3790 cm^{-1} belong to Al(VI)–OH on the (100) and reconstructed (110) facets, although we could not elucidate the individual contribution of each facet before. These new data provides an insight into the assignment of individual OH groups on alumina facets.

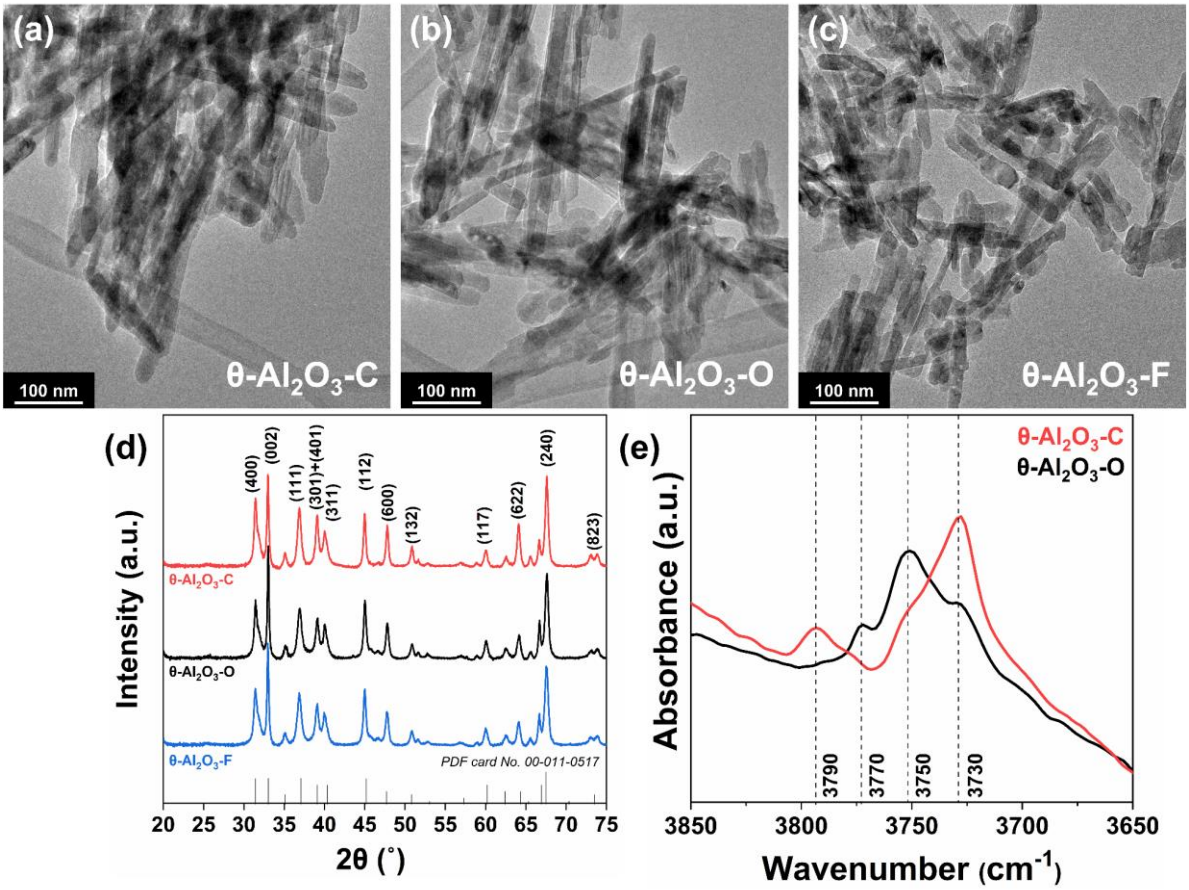

Figure 1 TEM images of (a) θ-Al_2O_3-C, (b) θ-Al_2O_3-O, (c) θ-Al_2O_3-F. (d) XRD diffraction pattern of θ-Al_2O_3-C, θ-Al_2O_3-O, and θ-Al_2O_3-F. (e) IR spectra of θ-Al_2O_3-C and θ-Al_2O_3-O.

The IR spectra displayed clear differences in the surface morphology of θ-Al_2O_3-C and θ-Al_2O_3-O/θ-Al_2O_3-F, whereas θ-Al_2O_3-O and θ-Al_2O_3-F showed similar surface OH bands. Meanwhile, the HRTEM images of θ-Al_2O_3-O and θ-Al_2O_3-F revealed that freeze-drying produced more textural mesoporous (voids), which changed the average interparticle distance between the crystals. This prompted us to investigate the stability of the three θ-Al_2O_3 samples, among which θ-Al_2O_3-F contained more voids. We previously reported that pure-phase θ-Al_2O_3 prepared via facet engineering of alumina shows enhanced stability and catalytic properties(*26*); however, its transformation into α-Al_2O_3 and stability against thermal stress were not investigated to date because such well-defined pure-phase and facet-engineered

materials were not available before. Thus, we conducted multimodal XRD, TEM, IR, and Brunauer–Emmett–Teller measurements to gain insight into this transformation (Figure 2–4, Figure S4–6), finding striking differences in the thermal behavior of these samples. The XRD patterns displayed in Figure 2a show peaks attributable to the (012) and (113) facets of α-Al_2O_3 at 2θ = 25.7° and 43.5°, respectively, indicating that the α phase started to develop in θ-Al_2O_3-C at 1140°C. At 1200°C, the α-phase peak was fully developed and that of the θ phase peak completely disappeared for θ-Al_2O_3-C. However, the XRD patterns of θ-Al_2O_3-F revealed that the signature peak of the α phase appeared at 1200 °C and that of the θ phase was still observed at 1260°C (Figure 2c). The transformation of θ-Al_2O_3-F to the α phase was complete at ~1300°C. Meanwhile, θ-Al_2O_3-O showed an intermediate trend between those of θ-Al_2O_3-C and θ-Al_2O_3-F (Figure 2b). To obtain more quantitative information, we normalized the amount of α phase using the peak intensity at 2θ = 25.7° for the samples treated at 1300°C (Figure 2d). When comparing θ-Al_2O_3-C and θ-Al_2O_3-F, the temperature at which the phase was completely transformed differs by ~100°C. The SA changes (Figure S3a) correspond well to this phase transformation because the transformation of θ phase into α phase is not topotactic and results in the formation of α-Al_2O_3 having lower surface area (SA). Notably, Al_2O_3-F exhibited a notable resistance to SA loss; treatment of Al_2O_3-F at 1200°C resulted in a SA loss of less than 20% with its value remaining above 40 m^2/g. Al_2O_3-O also showed a SA of ~30 m^2/g after such an extremely harsh treatment. These results prove that undoped alumina samples can still have notable thermal stability (up to 1260°C without full transformation into α-Al_2O_3). To the best of our knowledge, such thermally stable alumina samples have not been reported to date, without doping with rare-earths or barium. The SA of α-Al_2O_3-C decreased precipitously to 6 m^2/g at 1200°C, which is in line with a much easier formation of α-Al_2O_3, and stabilized at 5 m^2/g thereafter. The difference of the phase transformation temperature between the samples

despite their analogous initial rod-like morphology and pure θ phase can therefore be attributed to the different stability of the facets toward phase transformation (compare Al_2O_3-C with Al_2O_3-O and Al_2O_3-F) and different interparticle distances (between Al_2O_3-O and Al_2O_3-F).

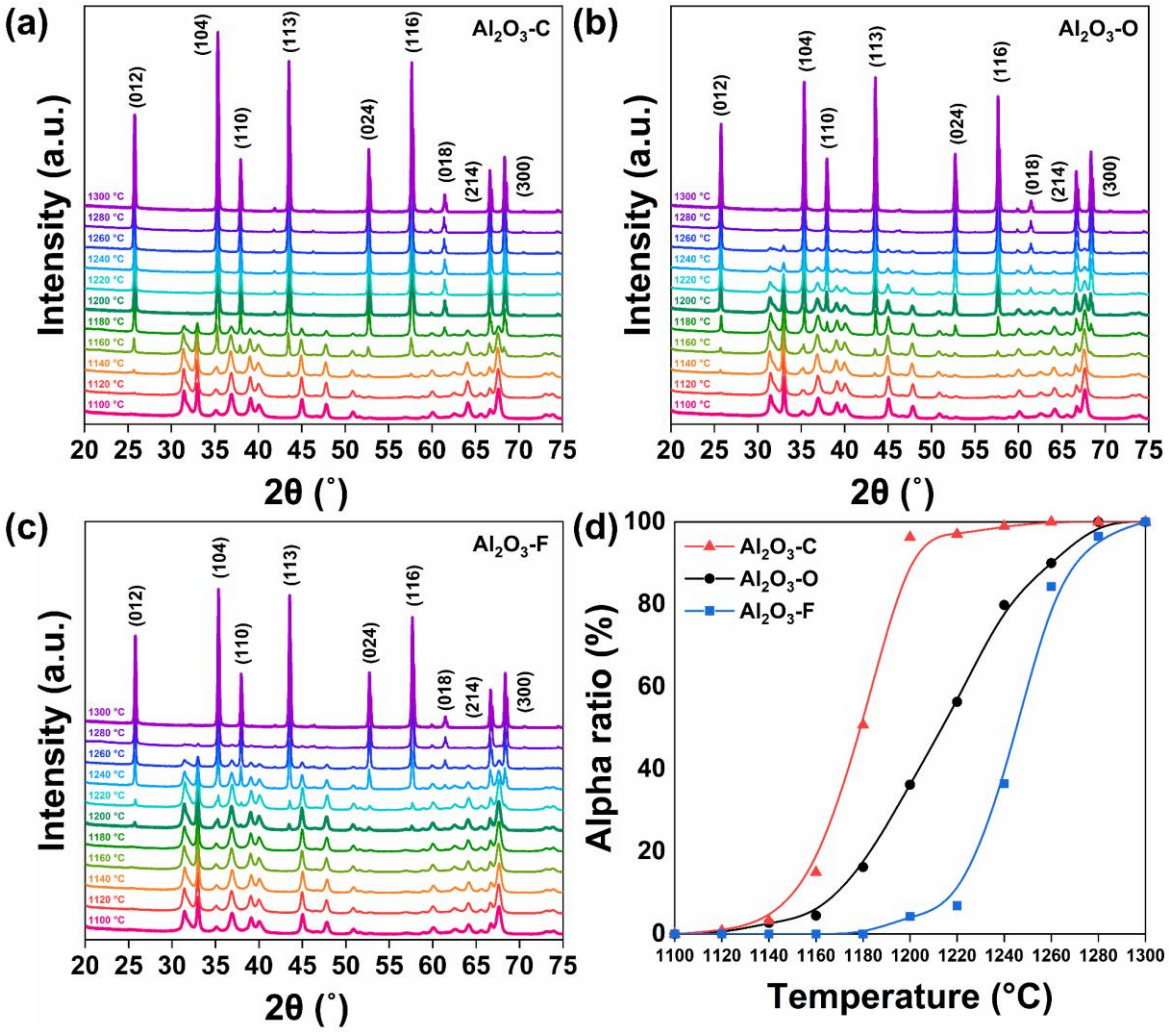

Figure 2 XRD diffraction patterns of (a) Al_2O_3-C, (b) Al_2O_3-O, and (c) Al_2O_3-F. (d) The ratio of α-phase as a function of temperature.

To investigate the effect of interparticle agglomeration on the phase transformation, we ground θ-Al_2O_3-F (denote as θ-Al_2O_3-F-G) and performed the same high-temperature treatment on the resulting sample. The temperature at which the phase transformation occurred decreased slightly, which suggests that this shift came partly from the decrease in the average interparticle

distance. Nevertheless, the ground sample showed a similar tendency to that of Al_2O_3-F (Figure S5a–c). Moreover, the surface property of the final product α-Al_2O_3-F did not change (Figure S5d). These results indicate that the surface property rather than particle agglomeration is the main factor affecting the phase transformation temperature.

To identify the morphology change and phase transformation, we studied the alumina samples used for the XRD analysis represented in Figure 2 via TEM. As shown in Figure 3, in the case of Al_2O_3-C, almost all the alumina particles maintained a rod-like shape at 1140°C. Meanwhile, the θ and α phases, which show a clearly different morphology, were heterogeneously distributed at 1180°C and 1220°C. No single small α-Al_2O_3 particles were observed in HRTEM/high-angle annular dark-field scanning transmission electron microscopy (HAADF-STEM) images even at a low conversion level (~10%). This suggests that the θ-to-α transformation does not proceed through gradual consumption of individual particles by an α-Al_2O_3 nucleus; instead, once a nucleus of α-Al_2O_3 is formed, it immediately consumes nearby alumina crystals with the concomitant formation of the α phase(*21*). In this respect, the interparticle distance musts play an important role in the transformation, which would explain the lower temperature of the phase transformation of θ-Al_2O_3-C compared with the other samples. At 1220°C, most of the particles were transformed into the α phase, but some of the θ phase still remained. At 1300°C, all particles were transformed into the α phase. Apart from the phase transformation, no further changes in the morphology of α-Al_2O_3 were observed upon high-temperature treatment, which suggests that no more sintering of the already formed α-Al_2O_3 occurred. This also explains the relatively large SA of the formed α-Al_2O_3 (Table S1) even after treatment at 1300°C for 10 h; the SA of α-Al_2O_3 is typically less than 1 m^2/g, whereas the SA of the present α-Al_2O_3 samples was ~5–8 m^2/g. The three samples showed the same

morphology-changing tendency during the phase transformation (Figure S6).

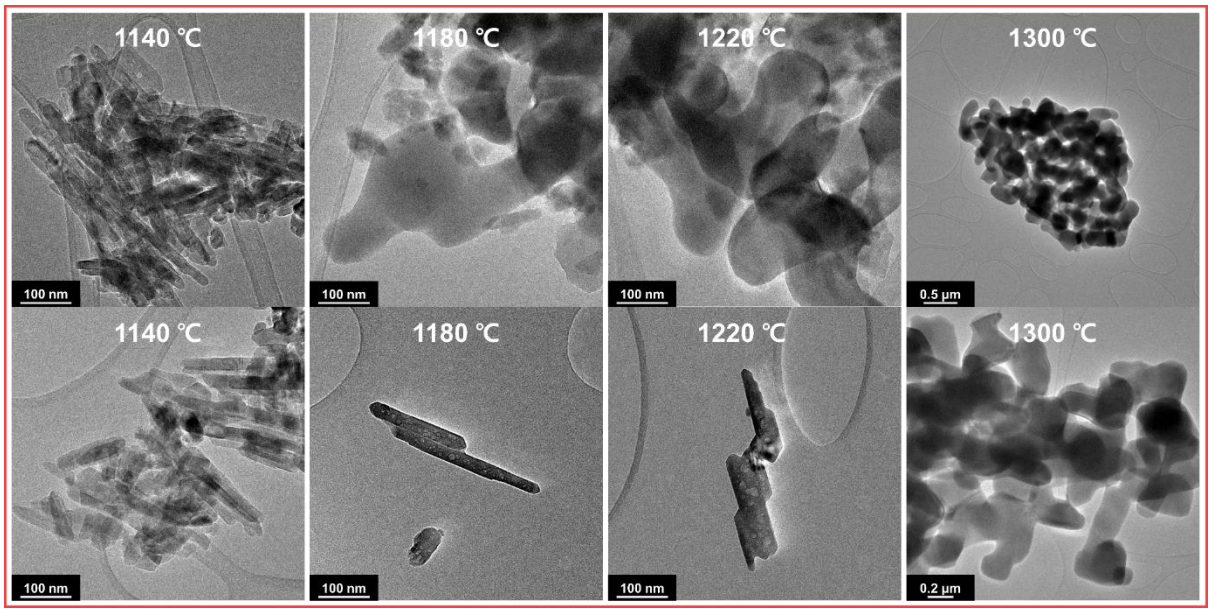

Figure 3 TEM images of Al_2O_3-C.

To confirm that the θ-to-α phase transformation does not occur within individual alumina nanocrystals, an individual Al_2O_3 particle on a high-temperature TEM grid was subjected to high-temperature treatment and observed via in situ TEM (Figure S7). During treatment at 1200°C, the single Al_2O_3 particle retained its shape but the volume shrank somewhat due to the coalescence of the internal pores. However, this single particle did not transform into α-Al_2O_3 after prolonged heating even at 1200°C. The fact that a single separated nanocrystalline particle does not undergo phase transformation provides direct, unambiguous evidence for the first time that interparticle contact is critical for the phase transformation of transition alumina to the α phase.

As mentioned above, the three samples show different surface properties; θ-Al_2O_3-C shows a dominant reconstructed (110) facet, whereas θ-Al_2O_3-O and θ-Al_2O_3-F primarily expose the (100) facet. Figure 4 shows the changes in the OH region of the IR spectra of the three samples

upon increasing the temperature. Interestingly, a significant OH band was observed at 3770 cm^{-1} in the IR spectra of α-Al_2O_3-C despite the drastic reduction of the SA(*15*). In contrast, that OH stretching band was virtually absent in the IR spectra of α-Al_2O_3-O and α-Al_2O_3-F. Despite their similar band position, the OH bands of α-Al_2O_3 might be due to different species to those of θ-Al_2O_3. In fact, careful inspection of the HRTEM and HAADF-STEM images revealed that the α-Al_2O_3-C particles exhibited a flatter morphology compared with the α-Al_2O_3-O/F particles, which showed a fibril-like morphology. This is most likely due to the presence of different dominant facets in α-Al_2O_3-C and α-Al_2O_3-O/F. Therefore, α-Al_2O_3 nanoparticles with different surface properties and a relatively high SA can be prepared from the same rod-like, pure-phase θ-Al_2O_3 samples. Our simple method enabled the synthesis of transition Al_2O_3 and α-Al_2O_3 materials with novel properties. Considering that Pd on alumina is one of the most important catalysts for industrial hydrocarbon oxidation, we loaded the materials prepared in this study with Pd and evaluated the performance of the resulting catalysts in hydrocarbon oxidation. We selected CH_4 as the most problematic hydrocarbon owing to its high greenhouse potential (about 27 times higher than that of carbon dioxide) and low tendency to undergo oxidation due to its apolar nature and absence of secondary C–H bonds.

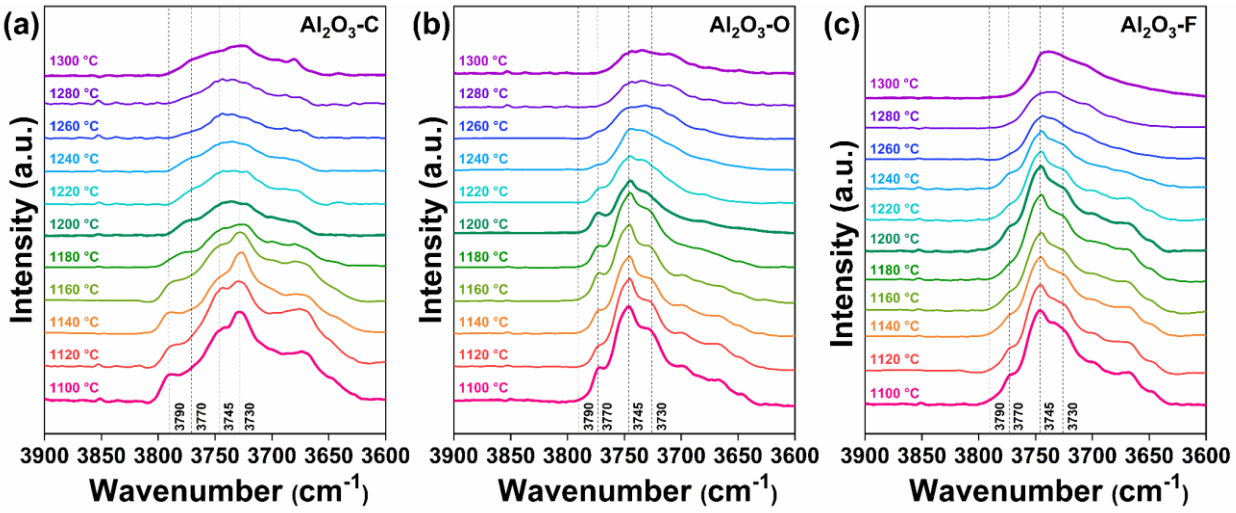

Figure 4 IR spectra of (a) Al_2O_3-C, (b) Al_2O_3-O, and (c) Al_2O_3-F from 1100 to 1300 °C with 20 °C intervals.

To investigate the effect of the different surface characteristics of the samples on the catalytic behavior, 0.1 wt% Pd was loaded on α-Al_2O_3-C and α-Al_2O_3-O, affording 0.1Pd/α-Al_2O_3-C and 0.1Pd/α-Al_2O_3-O, respectively. According to the TEM images shown in Figure 5a, b, and Figure S8, the size of Pd on α-Al_2O_3-C was around 3 nm and the size distribution was narrower than that of Pd on α-Al_2O_3-O, whose size was around 5 nm. However, the Pd size estimated using CO chemisorption measurements was 4 nm for α-Al_2O_3-C and 12 nm for α-Al_2O_3-O (Table S2). Thus, a considerable difference was observed between the size of Pd on α-Al_2O_3-O observed via TEM and that calculated using the CO chemisorption measurements, whereas Pd on α-Al_2O_3-C showed consistent results. This suggests the presence of large Pd particles on α-Al_2O_3-O, which could affect the dispersion significantly. The discrepancy observed for 0.1Pd/α-Al_2O_3-O is consistent with our previous reports(*15*), which demonstrated the occurrence of metal aggregation when the number of metal atoms exceeds that of the anchoring sites. This specific favorable interaction between metal and support was also confirmed by IR spectroscopy. Figure 5c displays the IR spectra of α-Al_2O_3-C, α-Al_2O_3-O, 0.1Pd/α-Al_2O_3-C,

and 0.1Pd/α-Al_2O_3-O. The band at 3770 cm^{-1} of α-Al_2O_3-C was notably reduced after Pd loading, which suggests that the corresponding OH groups were consumed as a result of their interaction with Pd(*15*). In contrast, the spectra of α-Al_2O_3-O and 0.1Pd/α-Al_2O_3-O showed no practical difference, demonstrating that the specific interaction of Pd with the OH groups producing the band at 3770 cm^{-1} results in a uniform metal loading and higher dispersion. This specific interaction and dispersion were confirmed by loading a higher Pd amount than that of the anchoring sites, which led to the formation of large metal clusters (Figure S9, 10, and Table S2).

To examine the influence of these differences in the Pd anchoring sites on the catalytic activity, we conducted CH_4 oxidation experiments using 0.1Pd/α-Al_2O_3-C and 0.1Pd/α-Al_2O_3-O. As shown in Figure 5d, the temperature at which the CH_4 conversion reached 50% was 10°C lower for 0.1Pd/α-Al_2O_3-C (439°C) than for 0.1Pd/α-Al_2O_3-O (449°C). However, the turnover frequency (TOF) and activation energy of 0.1Pd/α-Al_2O_3-C (112 kJ/mol) and 0.1Pd/α-Al_2O_3-O (114 kJ/mol) were almost the same (Figure S11 and Figure 5e). In particular, their activation energies were consistent with reported values(*23*).

Since the TOF of the two catalysts gradually increased with time, we performed DRIFTS experiments before and after the reaction to unveil the reason for the change in the catalytic activity (Figure S12). After 2 h of CH_4 oxidation reaction, the intensity of the band at 2140 cm^{-1}, which corresponds to surface partially oxidized Pd (PdO_x), increased slightly for 0.1Pd/α-Al_2O_3-C and 0.1Pd/α-Al_2O_3-O. This demonstrates that the Pd surface changes during the CH_4 oxidation reaction and corroborates the previous reports showing a correlation between surface PdO_x and the CH_4 oxidation activity(*27*).

In summary, our study provides a molecular-level understanding of the phase transformations

of alumina and a general method to prepare aluminas with advantageous thermal/catalytic properties.

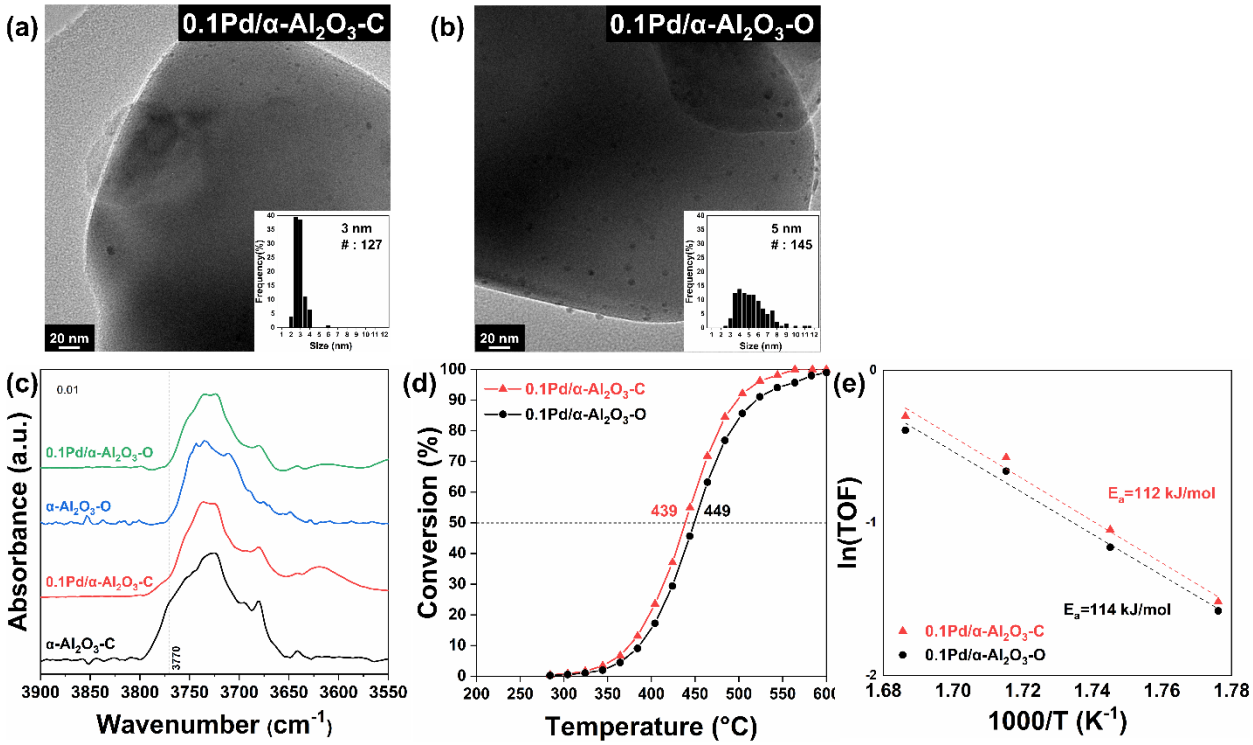

Figure 5 TEM images of (a) 0.1Pd/α-Al_2O_3-C and (b) 0.1Pd/α-Al_2O_3-O. (c) IR spectra of 0.1Pd/α-Al_2O_3-C and 0.1Pd/α-Al_2O_3-O, before and after Pd loading. (d) Temperature programmed reaction (TPR_x) profile of CH_4 oxidation on 0.1Pd/α-Al_2O_3-C and 0.1Pd/α-Al_2O_3-O. (e) Arrhenius plots for CH_4 oxidation with the reaction temperature of 290-320 ℃. The activation energy was calculated using TOF after 2 hours of reaction.

References

1. I. Levin, D. Brandon, Metastable alumina polymorphs: crystal structures and transition sequences. *Journal of the American Ceramic Society* **81**, 1995-2012 (1998).
2. S. Tauster, S. Fung, R. Baker, J. Horsley, Strong interactions in supported-metal catalysts. *Science* **211**, 1121-1125 (1981).
3. M. Boudart, Catalysis by supported metals. *Advances in catalysis* **20**, 153-166 (1969).
4. S. Rossignol, C. Kappenstein, Effect of doping elements on the thermal stability of transition alumina. *International Journal of Inorganic Materials* **3**, 51-58 (2001).
5. H. Schaper, E. Doesburg, L. Van Reijen, The influence of lanthanum oxide on the thermal stability of gamma alumina catalyst supports. *Applied Catalysis* **7**, 211-220 (1983).
6. H. Schaper, E. B. Doesburg, P. H. De Korte, L. L. Van Reijen, Thermal stabilization of high surface area alumina. *Solid State Ionics* **16**, 261-265 (1985).
7. H. P. Pinto, R. M. Nieminen, S. D. Elliott, Ab initio study of γ−Al_2O_3 surfaces. *Physical review B* **70**, 125402 (2004).
8. C. Wolverton, K. Hass, Phase stability and structure of spinel-based transition aluminas. *Physical review B* **63**, 024102 (2000).
9. G. Busca, The surface of transitional aluminas: A critical review. *Catalysis Today* **226**, 2-13 (2014).
10. H. Knözinger, P. Ratnasamy, Catalytic aluminas: surface models and characterization of surface sites. *Catalysis Reviews Science and Engineering* **17**, 31-70 (1978).
11. M. Digne, P. Sautet, P. Raybaud, P. Euzen, H. Toulhoat, Use of DFT to achieve a rational understanding of acid–basic properties of γ-alumina surfaces. *Journal of Catalysis* **226**, 54-68 (2004).
12. R. Guidetti, FT-IR Study of the Surface Properties of the Spinels $NiAl_2O_4$ and $CoAl_2O_4$ in Relation to Those of Transitional Aluminas. *Journal of Catalysis* **131**, 167-177 (1991).
13. B. Huggins, P. D. Ellis, Aluminum-27 nuclear magnetic resonance study of aluminas and their surfaces. *Journal of the American Chemical Society* **114**, 2098-2108 (1992).
14. A. Corma, Inorganic solid acids and their use in acid-catalyzed hydrocarbon reactions. *Chemical reviews* **95**, 559-614 (1995).

15. J. H. Kwak, J. Z. Hu, D. H. Kim, J. Szanyi, C. H. Peden, Penta-coordinated Al^{3+} ions as preferential nucleation sites for BaO on γ-Al_2O_3: An ultra-high-magnetic field ^{27}Al MAS NMR study. *Journal of Catalysis* **251**, 189-194 (2007).
16. C. Pecharroman, I. Sobrados, J. Iglesias, T. Gonzalez-Carreno, J. Sanz, Thermal evolution of transitional aluminas followed by NMR and IR spectroscopies. *The Journal of Physical Chemistry B* **103**, 6160-6170 (1999).
17. B. Deng, P. A. Advincula, D. X. Luong, J. Zhou, B. Zhang, Z. Wang, E. A. McHugh, J. Chen, R. A. Carter, C. Kittrell, J. Lou, Y. Zhao, B. I. Yakobson, Y. Zhao, J. M. Tour, High-surface-area corundum nanoparticles by resistive hotspot-induced phase transformation. *Nature Communications* **13**, 5027 (2022).
18. S. Lamouri, M. Hamidouche, N. Bouaouadja, H. Belhouchet, V. Garnier, G. Fantozzi, J. F. Trelkat, Control of the γ-alumina to α-alumina phase transformation for an optimized alumina densification. *Boletín de la Sociedad Española de cerámica y vidrio* **56**, 47-54 (2017).
19. S.R. Chauruka, A. Hassanpour, R. Brydson, K.J. Roberts, M. Ghadiri, H. Stitt, Effect of mill type on the size reduction and phase transformation of gamma alumina. *Chemical Engineering Science* **134**, 774-783 (2015).
20. A. P. Amrute, Z. Łodziana, H. Schreyer, C. Weidenthaler, F. Schüth, High-surface-area corundum by mechanochemically induced phase transformation of boehmite. *Science* **366**, 485-489 (2019).
21. P.-L. Chang, F.-S. Yen, K.-C. Cheng, H.-L. Wen, Examinations on the critical and primary crystallite sizes during θ-to α-phase transformation of ultrafine alumina powders. *Nano Letters* **1**, 253-261 (2001).
22. R. Bagwell, G. Messing, P. Howell, The formation of α-Al_2O_3 from θ-Al_2O_3: The relevance of a “critical size” and: Diffusional nucleation or ″synchro-shear”? *Journal of Materials Science* **36**, 1833-1841 (2001).
23. K. Murata, J. Ohyama, Y. Yamamoto, S. Arai, A. Satsuma, Methane Combustion over Pd/Al_2O_3 Catalysts in the Presence of Water: Effects of Pd Particle Size and Alumina Crystalline Phase. *ACS Catalysis* **10**, 8149-8156 (2020).
24. J. Lee, H. Jeon, D. G. Oh, J. Szanyi, J. H. Kwak, Morphology-dependent phase transformation of γ-Al_2O_3. *Applied Catalysis A: General* **500**, 58-68 (2015).

25. K. Khivantsev, N. R. Jaegers, J. H. Kwak, J. Szanyi, L. Kovarik, Precise Identification and Characterization of Catalytically Active Sites on the Surface of gamma-Alumina*. *Angewandte Chemie International Edition* **60**, 17522-17530 (2021).
26. J. Lee, E. J. Jang, H. Y. Jeong, J. H. Kwak, Critical role of (100) facets on γ-Al_2O_3 for ethanol dehydration: combined efforts of morphology-controlled synthesis and TEM study. *Applied Catalysis A: General* **556**, 121-128 (2018).
27. E. J. Jang, J. Lee, D. G. Oh, J. H. Kwak, CH_4 Oxidation Activity in Pd and Pt–Pd Bimetallic Catalysts: Correlation with Surface PdO_x Quantified from the DRIFTS Study. *ACS Catalysis* **11**, 5894-5905 (2021).

Keywords

alpha alumina, alumina, corundum, phase transformation

Acknowledgements:

Funding:

National Research Foundation (NRF) grant 2017R1A2B4007310 (SJJ, DGO, HNK, KHK, JHK)

Quickstarter Initiative at Pacific Northwest National Laboratory, under the Laboratory Directed research and Development Program at PNNL, a multiprogram national laboratory operated by Battelle for the U.S. Department of Energy. (KK)

AUTHOR INFORMATION

Corresponding Author

*Konstantin Khivantsev. Email : Konstantin.Khivantsev@pnnl.gov

*Libor Kovarik. Email : Libor.Kovarik@pnnl.gov

*Ja Hun Kwak. Email: jhkwak@unist.ac.kr

CRediT authorship contribution statement

Sejin Jang : synthesis and characterization of materials, data analysis, writing original draft.

Dong Gun Oh, Haneul Kim, **Kwang Hyun Kim** : catalyst characterization assistant.

Konstantin Khivantsev : conceptualization, infrared data collection, data analysis, writing & editing.

Libor Kovarik : in-situ TEM microscopy, data analysis, editing.

Ja Hun Kwak : supervision, conceptualization, resources, data analysis, review & editing, project administration.

All authors contributed to this work and have approved the final version of the manuscript.

Competing Interest:

The authors declare that they have no known competing financial interests or personal relationships that could have appeared to influence the work reported in this paper.

Data and materials availability:

All data are available in the manuscript or the supplementary materials.